

# Wetting Characteristics and Microscopic Synergistic Mechanism of Composite Surfactants on Coal Samples with Different Degrees of Metamorphosis

Limin Du,<sup>\*,§</sup> Jun Nian,<sup>\*,§</sup> Jinqi Fu, Jingchi Zhu, Hongfei Yu, Xiaoxia He, Chaowei Yang, and Lei Zhang



Cite This: *ACS Omega* 2025, 10, 6105–6118



Read Online

ACCESS |



Metrics & More

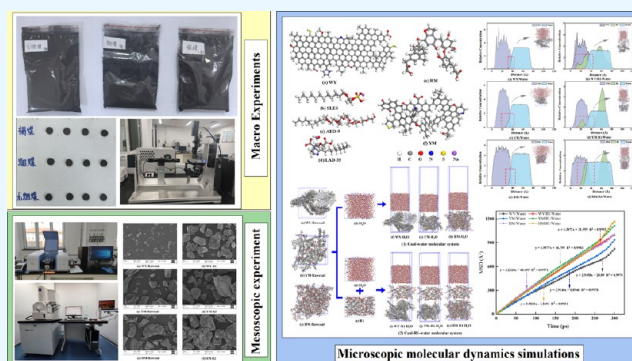


Article Recommendations



Supporting Information

**ABSTRACT:** This study investigates the effects of composite surfactants on the wettability of different coal types using a combination of macroscopic experiments, mesoscopic experiments, and microscopic molecular dynamics simulations, with coal samples of varying degrees of metamorphism as research subjects. First, contact angle and surface tension experiments were performed at the macroscopic level to determine the optimal concentration and ratio of the composite surfactants. The results showed that the composite solution formed by mixing SLES and AEO-9 in a 3:2 ratio significantly reduced both the surface tension of the solution and the contact angle of the coal samples at a mass concentration of 0.5 wt %. Second, the effects of the composite surfactants on the wetting properties of coal samples were analyzed at the mesoscopic level using scanning electron microscopy (SEM), Fourier transform infrared (FTIR) spectroscopy, and  $\zeta$ -potential measurements. The results revealed that the total content of hydrophobic groups ( $-\text{CH}_3$ ,  $-\text{CH}_2$ ,  $\text{C}=\text{C}$ ) in the coal molecules was significantly reduced after treatment with the composite solution, weakening the hydrophobicity of the coal samples. Additionally, the absolute value of the surface potential of the coal samples was significantly decreased, enhancing the aggregation tendency between coal particles. This facilitated the formation of larger agglomerated coal particles, which contributed to the settling of coal dust. Simultaneously, the cracks between coal particles promoted the penetration of aqueous solutions, aiding in the wetting of the coal seam. Finally, molecular dynamics simulations were conducted to analyze the synergistic wetting mechanism of the composite surfactants at the microscopic level. The results showed that the composite surfactant molecules were effectively adsorbed onto the surface of coal molecules, facilitating the movement of water molecules to the coal surface, increasing the diffusion coefficient of water molecules, and enhancing the interaction energy within the coal/composite surfactant/water system. These findings provide valuable insights for the development of new composite surfactants with wetting effects, offering significant potential for applications in mine dust control.



## 1. INTRODUCTION

Coal is the most abundant fossil fuel globally, and in China, it serves as the primary energy source, accounting for approximately 70% of the national energy supply.<sup>1–3</sup> With advancements in coal mining mechanization and automation, significant amounts of coal dust are generated during mining operations.<sup>4</sup> The hazards associated with coal dust are inevitable<sup>5</sup> and include environmental contamination, health risks to workers, equipment wear, and the potential for dust explosion accidents.<sup>6–8</sup> Thus, comprehensive management of coal dust pollution has become an urgent issue. Coal bed water injection, with its advantages of low equipment requirements, ease of use, low cost, and effective dust removal, is a key technology for mitigating and managing coal dust disasters.<sup>9–11</sup> However, due to the high hydrophobicity of coal dust and the high surface tension of pure water,<sup>12</sup> the efficacy of plain water in dust management is limited.<sup>13</sup> The addition of surfactants to water is a primary

method for enhancing the microstructural properties and wettability of coal.<sup>14,15</sup>

Currently, many researchers have investigated the effects of surfactants on the microstructure and wettability of coal.<sup>16–18</sup> Xu et al. examined the impact of SDBS and SDS on water injection in deep coal seams and found that both surfactants interacted with  $\text{Ca}^{2+}$ , resulting in precipitation that impeded water flow within the coal and hindered the improvement of wettability in deep coal seams.<sup>19–21</sup> Niu et al. combined molecular dynamics simulations and experiments to study the

Received: November 20, 2024

Revised: January 8, 2025

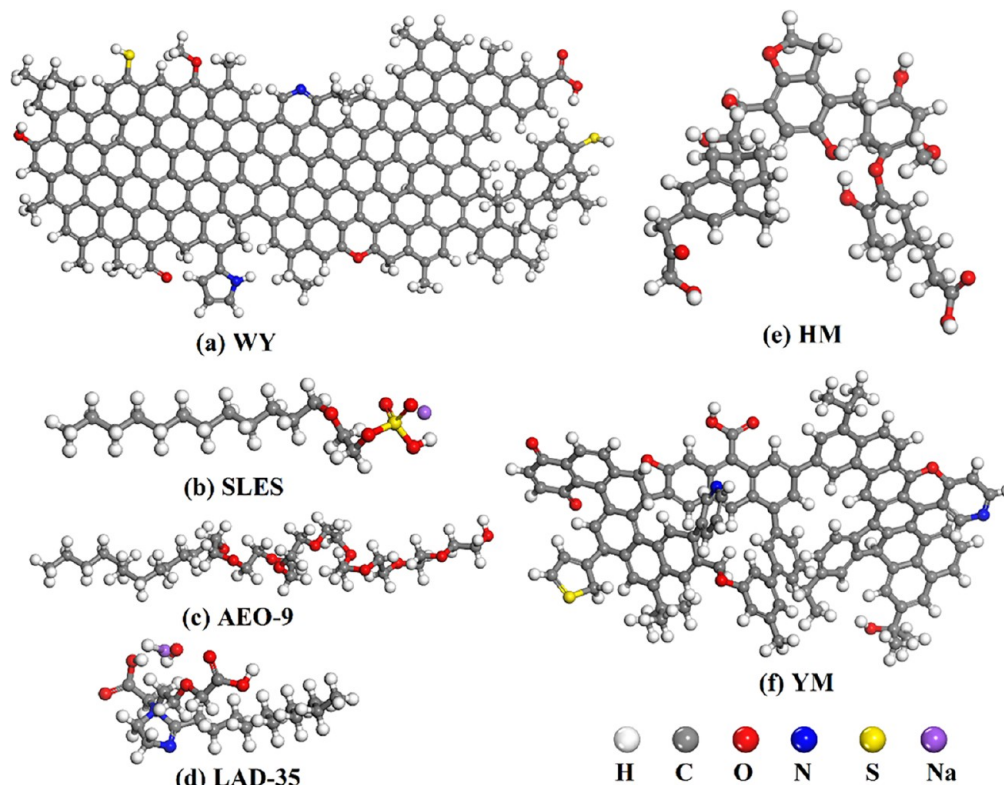
Accepted: January 13, 2025

Published: February 10, 2025



**Table 1. Industrial and Elemental Analyses of Coal Samples with Different Degrees of Deterioration**

coal sample	proximate analysis (%)				ultimate analysis (%)				
	Mad	Aad	Vad	FCad	Cdaf	Hdaf	Odaf	Ndaf	Sdaf
HM	10.39	4.33	37.91	47.37	67.52	3.88	26.73	1.24	0.63
YM	1.81	9.54	24.47	68.45	73.02	3.84	21.76	0.82	0.38
WYM	0.65	7.63	9.62	82.10	89.39	4.67	2.61	2.23	0.74

**Figure 1.** Coal and surfactant molecular structure.

adsorption and wetting process of APG-12 on coal molecules. They found that APG-12 readily adsorbed onto the coal surface, subsequently attracting surrounding water molecules, which significantly improved the wettability and inhibited coal dust.<sup>22,23</sup> Tian et al. reported that SDBS exhibited the best wetting performance when combined with IDS. This surfactant was more extensively adsorbed on the coal dust surface, increasing the surface porosity and specific surface area of bituminous coal, while also enhancing the proportion of oxygen-containing hydrophilic groups, thereby improving its wettability.<sup>19,24</sup> Gao et al. compared the effects of two nonionic surfactants, C12G2 and C12E7, on the surface wettability of lignite, and found that the hydroxyl-containing C12G2 enhanced the hydrophilicity of lignite.<sup>25,26</sup> Chen et al. investigated the effects of AEO-9 on the wettability of anthracite through both experiments and simulations. They discovered that AEO-9 increased the migration rate of water molecules, promoted the movement of a large number of water molecules to the anthracite surface, thickened the water molecule layer, and strengthened the anthracite/water interaction.<sup>27–29</sup> Meng et al. analyzed the effect of surfactants with different hydrophilic structures on the wettability of bituminous coal, concluding that surfactants containing higher amounts of oxygen and nitrogen in their hydrophilic structures were more effective in modulating the wettability of bituminous coal.<sup>30–32</sup> Jing et al. studied the

effect of different surfactant blends on the wettability of bituminous coal, finding that a compound solution of SDS and CAB-50 exhibited a better synergistic effect, which effectively reduced the contact angle, increased the relative concentration of water molecules on the coal surface, improved dust suppression efficiency, and significantly enhanced the wettability of bituminous coal.<sup>33–35</sup> In summary, while some preliminary studies on the wettability of coal have been conducted, research on the effect of compound surfactants on the wettability of different coal types remains limited due to the complex physical and chemical structures of various coal species.

In this study, anthracite, bituminous coal, and lignite with varying degrees of metamorphism were selected as the research subjects to investigate the effects of compound surfactants on the wettability of different coal species. This was achieved through a combination of macroscopic experiments, mesoscopic analysis, and microscopic molecular dynamics simulations. First, the influence of different surfactant compound ratios on the wettability of the three coal samples was assessed using contact angle and surface tension measurements to identify the optimal compound formulation and surfactant concentration. Second, the effects of the compound surfactants on the surface element and functional group changes of the coal samples were analyzed through scanning electron microscopy (SEM), Fourier transform infrared (FTIR) spectroscopy, and  $\zeta$ -potential measure-

ments. Finally, molecular dynamics simulations were conducted to model the coal/water and coal/compound surfactant/water systems. The interaction between these systems was analyzed in terms of interaction energy, relative concentration distribution, and mean square displacement (MSD) of water molecules, which further elucidated the microscopic mechanism of the synergistic wetting effect of the compound surfactants on coal dust. The study of the wettability of coal dust by compound surfactants provides insights into the development of more effective coal dust inhibitors, enhances the wettability of water injection in coal seams, reduces coal dust dispersion, improves the working environment, and has significant application value for mine dust control. Improving the wettability of coal enhances reaction efficiency and conversion rates, promotes the efficient and clean utilization of coal resources, and offers technical support for the deep processing and comprehensive utilization of coal.

## 2. EXPERIMENTS AND SIMULATIONS

**2.1. Experimental Materials.** The coal samples used in the experiments were sourced from different mining regions in China, listed in order of decreasing metamorphism: Ordos lignite (HM), Shouyang bituminous coal (YM), and Jincheng anthracite (WYM). The coal samples were crushed using a ball mill, then sieved through a vibrating screen with a 200-mesh sieve. The screened coal dust samples were placed in a vacuum desiccator at 50 °C for 24 h, after which they were stored in the desiccator for later use. The results of industrial and elemental analyses for the three coal samples, which exhibit varying degrees of metamorphism, are presented in Table 1. It can be observed that with increasing metamorphism, the carbon content in the coal gradually increases, while the oxygen content decreases.

Based on previous studies on wetting agents conducted by our group, anionic surfactant sodium lauryl sulfate (SLES, 70%, Usoft), nonionic surfactant fatty alcohol polyoxyethylene ether (AEO-9, 99%, Usoft), and amphoteric surfactant sodium lauroyl amphoteric bis(acetate) (LAD-35, 35%, Usoft) were selected for the experiments. The reagents were purchased from Shandong Usoft Chemical Technology Co., and their molecular structures are shown in Figure 1. In prior single-solution experiments, the critical micelle concentration (CMC) of each solution was determined to be 0.5 wt %. Therefore, in this study, an orthogonal experimental design was not applied. Instead, the CMC concentration was adopted as the concentration of the mixed surfactant solutions. The selected surfactants were blended in mass ratios of 5:0, 4:1, 3:2, 2:3, 1:4, and 0:5, resulting in the preparation of composite surfactant solutions R1 (SLES:AEO-9), R2 (AEO-9:LAD-35), and R3 (SLES:LAD-35). Tap water was used as the solvent to simulate real-world coal mine conditions, and all experiments were conducted at room temperature.

**2.2. Experimental Methods and Equipment.** **2.2.1. Surface Tension and Contact Angle.** Two grams of coal powder were evenly distributed in the center of the tablet press bushing and subjected to a pressure of 15 MPa for 3 min. The coal powder was then pressed into a flake with a smooth surface, measuring 40 mm in diameter and 5 mm in thickness. Composite surfactant solutions with varying mass ratios were prepared, and the surface tension of these solutions was measured using an SDC-350 automatic contact angle/surface tension tester. The contact angles of different coal samples were

also determined with this instrument. Each set of experiments was repeated three times, and the average value was calculated.

**2.2.2. Scanning Electron Microscope Experimental Measurements.** A scanning electron microscope (SEM, ESCALAB 250Xi) was employed to acquire images in high vacuum mode for observing the morphology and surface ultrastructure of various solid materials.<sup>36</sup> A 2 g sample of coal powder was weighed and mixed with an equal volume of different composite surfactant solutions. The mixture was allowed to stand for 48 h to ensure adequate wetting of the coal samples, followed by drying in a vacuum oven at 40 °C for 48 h. A small portion of the coal sample was then taken for plating experiments. The bonding and adsorption effects of the surfactant on the surface of anthracite coal were observed at a magnification of  $\times 2000$ .

**2.2.3. FTIR Spectroscopy Analysis.** The infrared spectra of coal samples with varying degrees of metamorphism were measured using an INVENIO R Fourier transform infrared spectrometer.<sup>37</sup> Initially, pure KBr was used to collect the background spectrum as a baseline reference. Next, KBr was mixed with coal dust in a 150:1 ratio and thoroughly ground. The resulting mixture was then compressed into transparent flakes with a thickness ranging from 0.1 to 1.0 mm using a tablet press. Finally, the samples were placed in the sample chamber of the FTIR spectrometer for analysis, with a scanning range of 4000–400  $\text{cm}^{-1}$  and a resolution of 4  $\text{cm}^{-1}$ . Each coal sample was scanned 32 times.

**2.2.4. Zeta Potential Measurement.** The  $\zeta$ -potential of coal dust with varying degrees of deterioration in the composite surfactant solution was measured using a  $\zeta$ -potential meter (Nanobrook 90Plus PALS). A 0.5 g sample of coal was added to 100 mL of composite surfactant solution and diluted to a 0.5% suspension. The suspension was then thoroughly dispersed using ultrasonic stirring for 60 s and allowed to stand for 24 h. Subsequently, the supernatant was carefully collected for  $\zeta$ -potential measurement. As detailed in Section 2.1, a 0.5% concentration of the composite surfactant solution provided better wettability and a more uniform distribution of coal sample particles. At this concentration, the coal particles exhibited relatively stable motion in the electric field, ensuring a sufficient number of coal particles for measurement.<sup>38,39</sup> Additionally, this concentration minimized the interference from interparticle interactions, thereby enhancing the accuracy and repeatability of the  $\zeta$ -potential measurements.

**2.3. Molecular Dynamics Simulation.** In this study, typical Wender and Wiser models were selected to construct the macromolecular structures of anthracite, lignite, and bituminous coal.<sup>40,41</sup> Molecular dynamics simulations were performed using Materials Studio 2020 software. First, the molecular structures of water, surfactant, and coal were constructed, followed by geometry optimization and annealing to obtain the minimum energy configurations. Next, 1000 water molecules, 10 surfactant molecules, and 15 coal molecules were randomly introduced into a cell with dimensions of 35 Å  $\times$  35 Å using the Amorphous Cell module. The coal/water and coal/surfactant–water systems were then modeled using the Build Layer tool. A vacuum layer of 30 Å was added along the z-axis to eliminate periodic boundary conditions. The three systems were subsequently subjected to geometry optimization and multiple annealing steps. Finally, molecular dynamics simulations of the optimized systems were carried out using the Forcite module, with an NVT ensemble, a temperature of 298 K, a time step of 1.0 fs, and a simulation duration of 300 ps.<sup>42</sup> The molecular

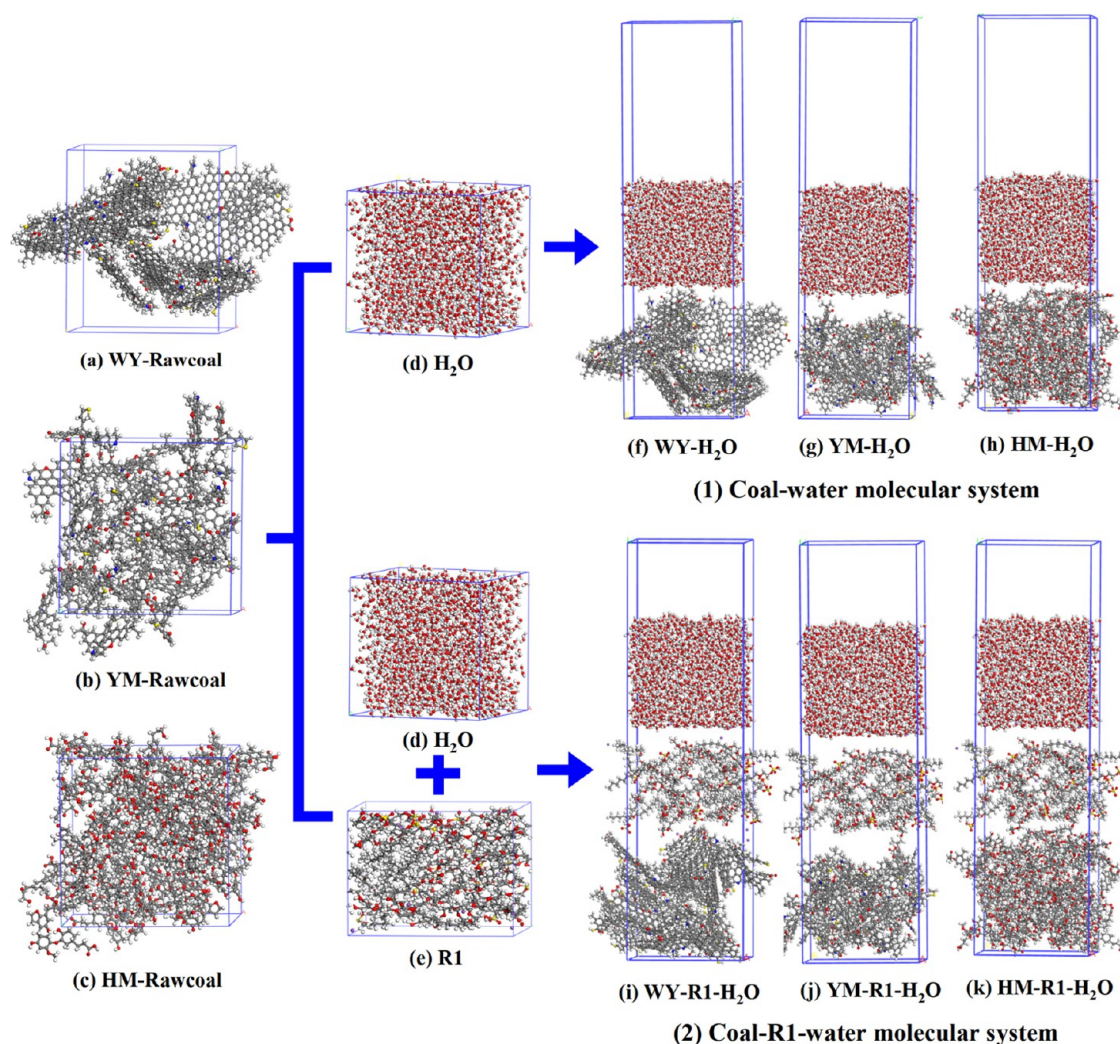


Figure 2. Initial configurations of different molecular systems.

models and the molecular dynamics simulation process are shown in Figures 1 and 2, respectively.

### 3. RESULTS AND DISCUSSION

**3.1. Analysis of Experimental Results.** **3.1.1. Surface Tension.** Surface tension is a key parameter for characterizing the wetting ability of a liquid.<sup>43</sup> The surface tension of composite surfactants at different mass ratios was determined through surface tension measurements, as shown in Figure 3. It is observed that the surface tension of the R1 composite solution is lower than that of the individual surfactants. Specifically, the surface tension of the anionic surfactant SLES combined with the nonionic surfactant AEO-9 at a 3:2 mass ratio is 26.246 mN/m, which is 13.42 and 19.60% lower than that of the individual surfactants, indicating a better synergistic effect between the anionic and nonionic surfactants. This suggests that the combination of anionic and nonionic surfactants leads to enhanced synergistic effects. This is attributed to the negative charge of the anionic surfactant molecules, which results in strong electrostatic repulsion between molecules, thereby increasing the molecular spacing. The nonionic surfactant AEO-9, with its higher oxygen-containing functional groups, interacts easily with water molecules to form hydrogen bonds, which can entangle with the anionic surfactants, filling intermolecular gaps and reducing the surface tension of the

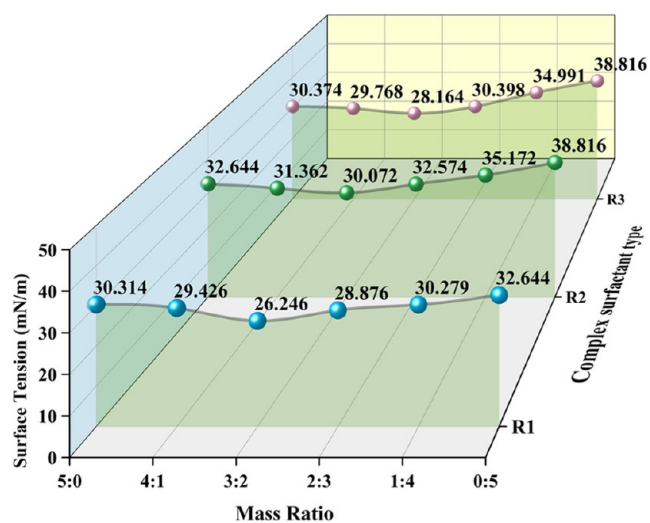
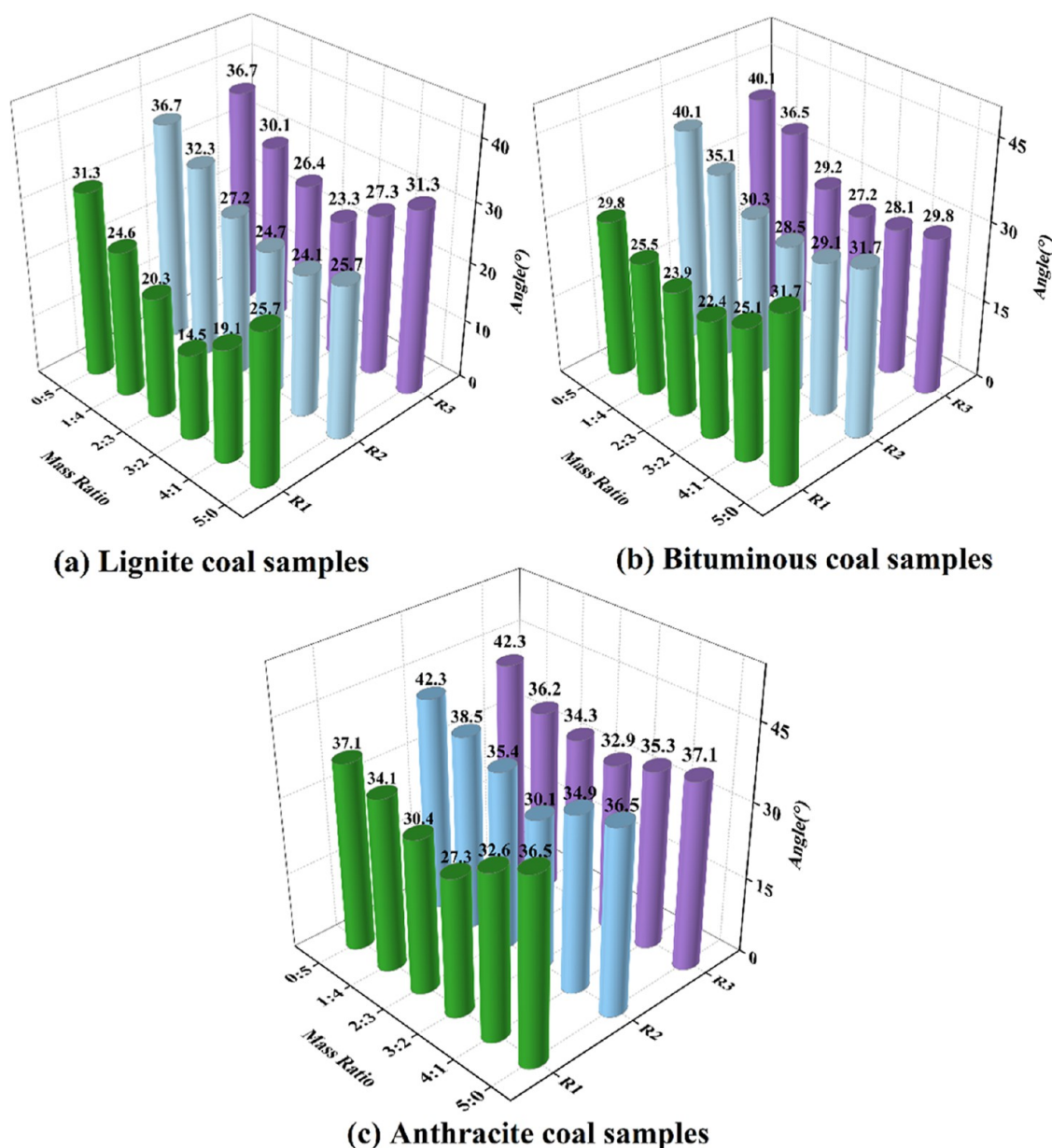


Figure 3. Surface tension of composite surfactants at different mass ratios.

solution. Although the other two composite formulations did not achieve lower surface tension than the lowest value of the single component solutions, they still reduced the surface tension to some extent. The minimum surface tension values of



**Figure 4.** Contact angle values of composite surfactants with different mass ratios in different coal samples.

the R2 and R3 composite solutions at a 3:2 mass ratio were 30.072 and 28.164 mN/m, respectively, both lower than the surface tension of the individual surfactant solutions. This indicates that the composite surfactants are effective in lowering the surface tension, thereby enhancing their wetting ability on coal seams.

**3.1.2. Contact Angle.** The contact angle experiment provides a microscopic perspective for comparing the diffusion and wetting abilities of liquids on solid surfaces.<sup>44</sup> Figure 4 presents the contact angle values of different mass ratios of compound surfactants on three coal samples. The data indicate that the contact angles of the three composite solutions are lower than that of the single surfactant solution. The contact angle of anthracite in a single SLES solution is 34.501°, while the contact angle for the nonionic AEO-9 at a 3:2 ratio is 27.301°, a 20.87% reduction compared to the single surfactant solution. The minimum contact angle of bituminous coal in the single surfactant solution is 25.858°, while the minimum contact angle

in the R1 compound solution is 19.575°, a decrease of 24.29%. For lignite, the minimum contact angle in the single surfactant solution is 20.798°, whereas in the R1 solution, it is 14.545°, resulting in a reduction of 30.17%. These results suggest that compound surfactants improve the wetting performance of coal samples. Combining the results from the surface tension and contact angle experiments, it is evident that the R1 compound solution with a mass ratio of 3:2 and a concentration of 0.5 wt % provides the best wetting effect for coal samples with varying degrees of deterioration. Future work will focus on using this R1 compound solution to treat coal samples with different deterioration levels and analyze its wetting mechanism.

**3.1.3. Scanning Electron Microscopy.** SEM experiments can provide insights into the wetting and binding properties of the solution on coal sample surfaces at a microscopic level.<sup>45</sup> Figure 5 presents the microscopic morphology of coal samples with varying degrees of metamorphism, treated with a composite surfactant, at a magnification of 2000 times. The untreated raw

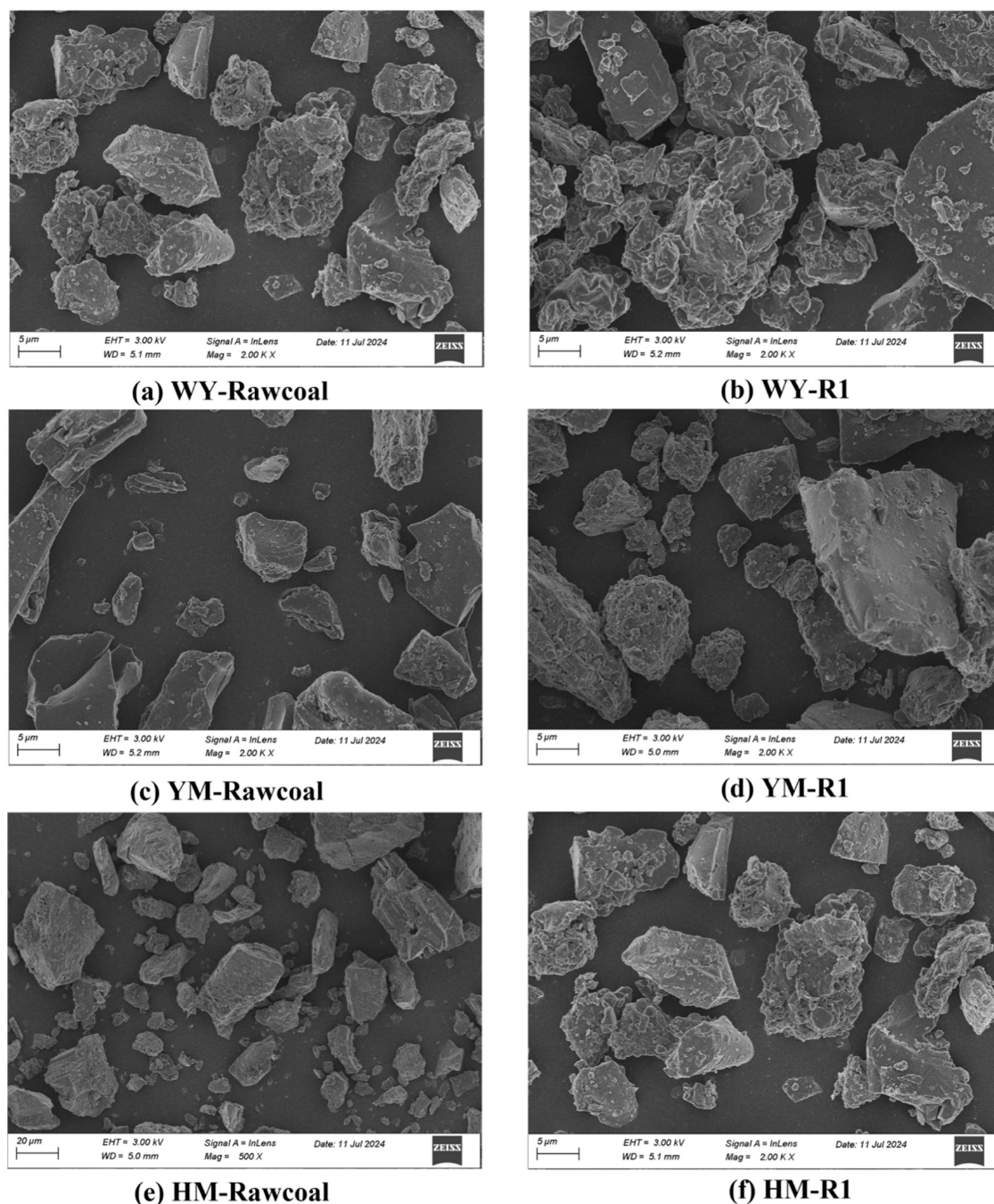


**Figure 5.** Micromorphological images of coal samples with different degrees of metamorphism after treatment with surfactant complexes at 2000 times magnification.

coal sample exhibits numerous small coal particles on its surface, with a relatively loose distribution of these particles. In contrast, the surface of the coal sample treated with the composite surfactant shows aggregation of many coal particles. Small particles adsorb and bind to larger coal particles under the action of the composite surfactant, and the interactions between the larger and smaller particles form clusters. These clusters facilitate settling and reduce dust hazards. Additionally, the coal clusters contain abundant pore structures, which promote solution penetration during water injection into the coal seam and, to some extent, enhance the wettability of the coal seam.

**3.1.4. FTIR Spectra.** Figure 6 presents a comparison of FTIR spectra for coal samples with different metamorphic degrees in

the region of  $1000\text{--}1800\text{ cm}^{-1}$  after treatment with the R1 solution. This region includes oxygen-containing functional groups, which consist of seven types: Si–O–Si stretching vibration, C–O–C stretching vibration, C–O stretching vibration,  $-\text{CH}_3$  symmetric bending vibration,  $-\text{CH}_3$  and  $-\text{CH}_2$  antisymmetric bending vibrations, C=C stretching vibration, and C=O stretching vibration.<sup>46</sup> Figure 7 illustrates the percentage change in the area of oxygen-containing functional groups for the three coal samples after treatment with the R1 composite solution. It can be observed that the total content of hydrophobic groups ( $-\text{CH}_3$ ,  $-\text{CH}_3$  &  $-\text{CH}_2$ , C=C) in lignite coal decreased from 48 to 39% after R1 treatment. In bituminous coal, the content of hydrophobic groups decreased

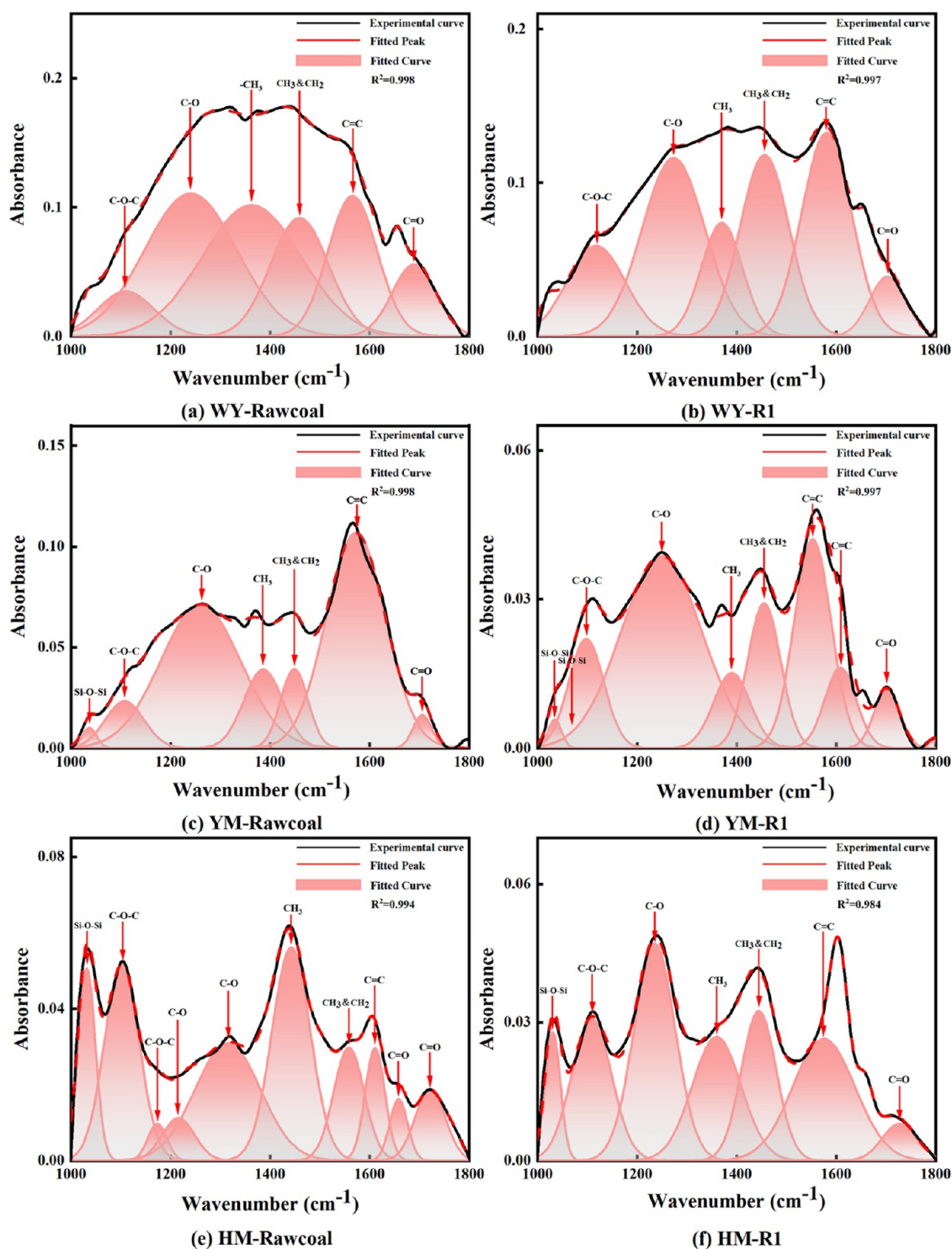


**Figure 6.** Comparison of FTIR spectra of coal samples with different degrees of metamorphism in the 1000–1800  $\text{cm}^{-1}$  region after treatment with R1 solution.

from 54 to 45%, while in anthracite, the hydrophobic group content decreased from 67 to 54%. Overall, the trend shows a decrease in hydrophobic group content in all three types of coal samples treated with R1 composite solution, while the total peak area of hydrophilic groups increases. This is attributed to the fact that anionic and nonionic molecules, which are rich in hydrophilic groups such as  $-\text{OH}$ ,  $-\text{COOH}$ ,  $\text{C}-\text{O}-\text{C}$ ,  $\text{COO}^-$ , and  $-\text{SO}_3\text{H}$ , adsorb onto the coal surface during coal dust infiltration. This adsorption alters the functional group

composition of the coal, ultimately leading to an increase in the content of hydrophilic groups and a decrease in the content of hydrophobic groups.

Figure 8 presents a comparison of the FTIR spectra of coal samples with varying degrees of metamorphism in the 2800–3000  $\text{cm}^{-1}$  region after treatment with the R1 solution. This region corresponds to the aliphatic functional group structure, which includes four main types:  $-\text{CH}_2$  symmetric stretching,  $-\text{CH}$  stretching,  $-\text{CH}_2$  antisymmetric stretching, and  $-\text{CH}_3$

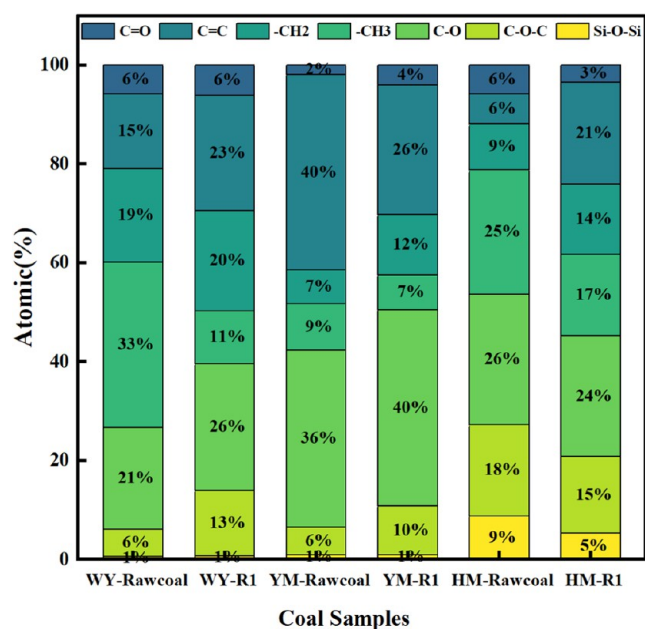


**Figure 7.** Percentage change in the area of oxygen-containing functional groups of the three coal samples after treatment with the R1 composite solution.

antisymmetric stretching.<sup>47</sup> It can be observed that these aliphatic functional groups are reduced to varying extents after treatment with composite surfactants, with the reduction of CH<sub>2</sub> and CH<sub>3</sub> groups being more pronounced. To further investigate the evolution of the aliphatic hydrocarbon structure in the coal samples after surfactant treatment, the following formula was employed to characterize the length and branching degree of the aliphatic chains.<sup>48</sup>

$$\frac{A(\text{CH}_2)}{A(\text{CH}_3)} = \frac{A_{2924\text{cm}^{-1}}}{A_{2954\text{cm}^{-1}}} \quad (1)$$

where  $A_{2924\text{cm}^{-1}}$  and  $A_{2954\text{cm}^{-1}}$  represent the peak areas of  $-\text{CH}_2$  and  $-\text{CH}_3$  groups near 2920 and 2950  $\text{cm}^{-1}$ , respectively.

The results of the operations are presented in Table S1. It can be observed that the CH<sub>2</sub>/CH<sub>3</sub> ratio slightly increased for different coal samples treated with R1 solution, indicating the presence of longer and less branched aliphatic chains in the coal samples. This is primarily attributed to the complex surfactant solution of anionic and nonionic components, which increased the cracks in the coal structure, allowing some aliphatic structures to overcome spatial constraints and be released. These released structures then combine with lipids to form longer fatty chains with fewer branches. Furthermore, it is noted that the  $A(\text{CH}_2)/A(\text{CH}_3)$  ratio gradually decreased with increasing deterioration, suggesting that as the deterioration progressed, the aliphatic chain length decreased, and the number of branched chains increased. This indicates that the degree of aliphatic chain breakage is higher in coal samples with a higher degree of deterioration.

**3.1.5. Zeta Potential.** In addition to changes in the content of functional groups, the adsorption of surfactants may also influence the surface potential of coal dust.<sup>49</sup> Figure 9 illustrates the effect of different solutions on the  $\zeta$ -potential of coal particles. In pure aqueous solution, the  $\zeta$ -potentials of anthracite, bituminous coal, and lignite were  $-40.03$ ,  $-51.69$ , and  $-62.58$  mV, respectively. It can be observed that in aqueous solution, the  $\zeta$ -potentials of all coal surfaces were negative, with

the absolute value of the  $\zeta$ -potential gradually decreasing as the degree of coalification increased. This is primarily because carboxyl and hydroxyl groups on the coal surface readily dissociate, generating negatively charged ions, which impart a negative charge to the coal surface.<sup>50</sup> As the degree of coalification increases, the number of negatively charged functional groups on the coal surface decreases, resulting in an increase in the surface  $\zeta$ -potential. After the addition of the composite surfactant, the  $\zeta$ -potential in the solution changed. The  $\zeta$ -potentials of anthracite, bituminous coal, and lignite in the composite solution were 25.06,  $-34.72$ , and  $-40.09$  mV, respectively, with the absolute  $\zeta$ -potential values decreasing by 35.93, 32.83, and 37.39% compared to those in the single aqueous solution. This indicates that under the influence of the composite surfactant solution, the coal surface remained negatively charged. Notably, under the action of the composite surfactant solution, the absolute  $\zeta$ -potential values of the coal samples showed a decreasing trend. This is because the anionic and nonionic interactions of the R1 composite surfactant enhanced its adsorption on coal particles, altering the interfacial properties of the coal/water interface. As a result, the hydrophobic tail chains of the surfactant were more widely adsorbed on the coal surface, while the hydrophilic groups were exposed to the aqueous phase, thus increasing the hydrophilicity of the coal dust. The lower absolute  $\zeta$ -potential values indicate that the aggregation ability between coal dust particles was enhanced, which is more favorable for dust settling.

**3.2. Molecular Simulations.** **3.2.1. Interaction Energy Calculations.** The interaction energy quantifies the strength of the interaction between the surfactant and coal.<sup>31</sup> It is calculated as follows

$$E_{\text{int}} = E_{\text{total}} - (E_x + E_{\text{coal}}) \quad (2)$$

$E_{\text{int}}$  represents the adsorption energy between water/surfactant and coal molecules;  $E_{\text{total}}$  is the total conformational energy of the water/surfactant/anthracite system;  $E_x$  denotes the conformational energy of the water or water/surfactant system; and  $E_{\text{coal}}$  corresponds to the conformational energy of the coal molecules.

The calculated results are presented in Table 2. The interaction energies of anthracite, bituminous coal, and lignite with a single water system were  $-258.48$ ,  $-380.32$ , and  $-500.89$  kcal/mol, respectively. Negative values indicate spontaneous adsorption, where a larger absolute value corresponds to stronger adsorption. The adsorption performance of the three coal samples follows the order: lignite > bituminous coal > anthracite. This suggests that the surface hydrophilicity of anthracite is inferior to that of bituminous coal and lignite, making it less likely to interact with water molecules. This difference primarily arises from the molecular structures of the coal types. Anthracite, as a high-rank coal, has fewer polar oxygen-containing functional groups on its surface and a significant number of hydrophobic sites, resulting in stronger overall hydrophobicity. In contrast, lignite contains more oxygen-containing functional groups in its macromolecular structure, such as  $-\text{OH}$ ,  $-\text{COOH}$ ,  $\text{C}-\text{O}-\text{C}$ ,  $\text{COO}^-$ , which facilitate interactions with water molecules. Upon the addition of the compound surfactant R1, the interaction energies of the three systems were  $-528.74$ ,  $-604.66$ , and  $-1016.16$  kcal/mol, respectively. This indicates that the absolute values of the interaction energies for the coal/surfactant/water systems were higher than those for the coal/water systems. The presence of the compound surfactant intensified water molecule dynamics

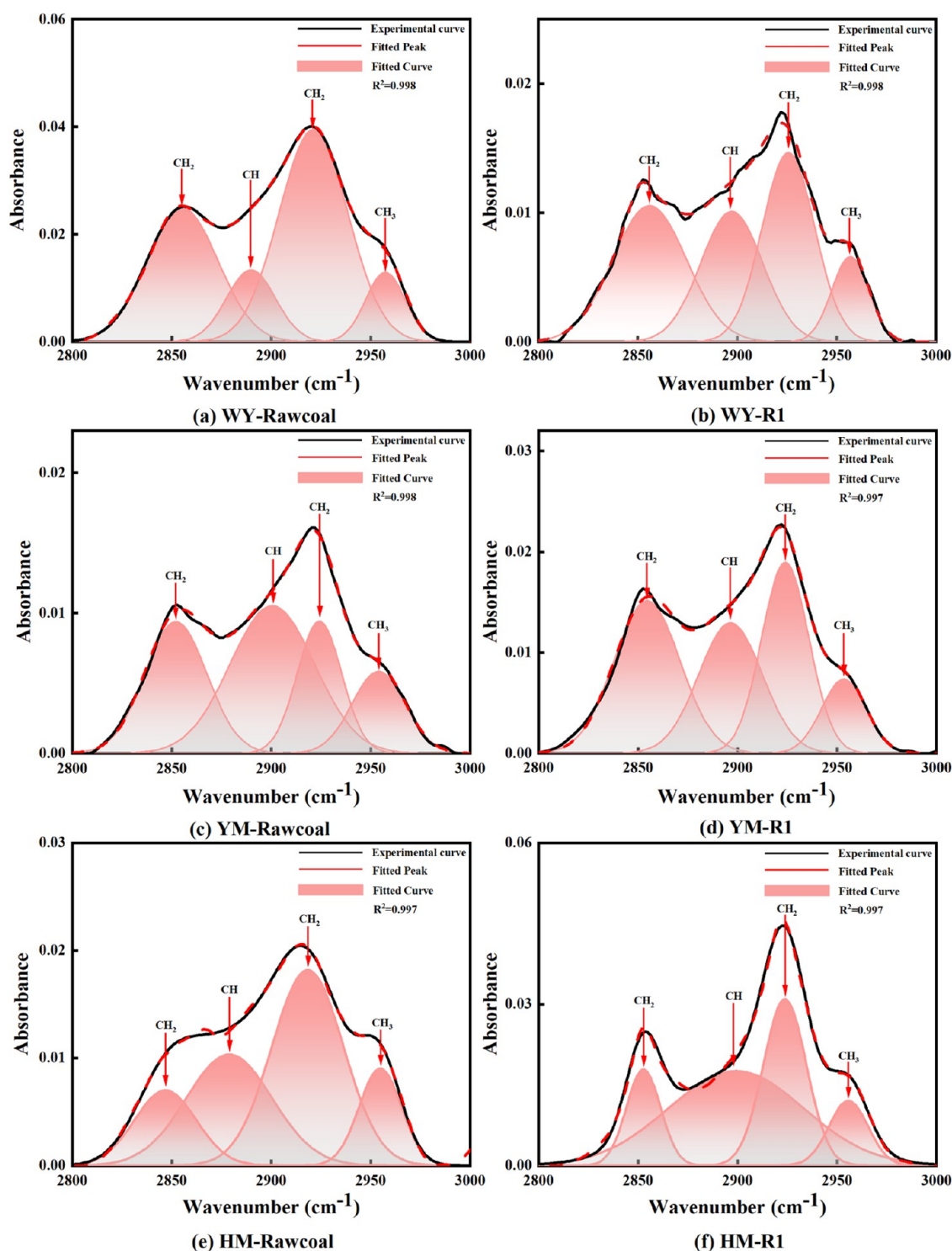


**Figure 8.** Comparison of FTIR spectra of coal samples with different degrees of metamorphism in the region of 2800–3000  $\text{cm}^{-1}$  after treatment with R1 solution.

and increased the contact between water and coal, leading to more stable water molecule aggregation.<sup>51</sup> This effect can be attributed to the synergistic action of the anionic-nonionic compound surfactant, which enhances dipole-ion interactions among polar head groups, reduces electrostatic repulsion between surfactant molecules, and facilitates adsorption between water and coal molecules. Consequently, the interaction between the polar hydrophilic groups of the

surfactant and water molecules is strengthened, improving the hydrophilicity of the coal samples.

**3.2.2. Relative Concentration Distribution Analysis.** Figure 10 illustrates the concentration distribution of each component along the Z-axis in various systems, providing a quantitative assessment of the adsorption capacity of the composite surfactant R1 and the structural parameters of the adsorption layer. The relative concentration distribution of coal molecules across different systems exhibits minimal variation,<sup>52</sup> primarily

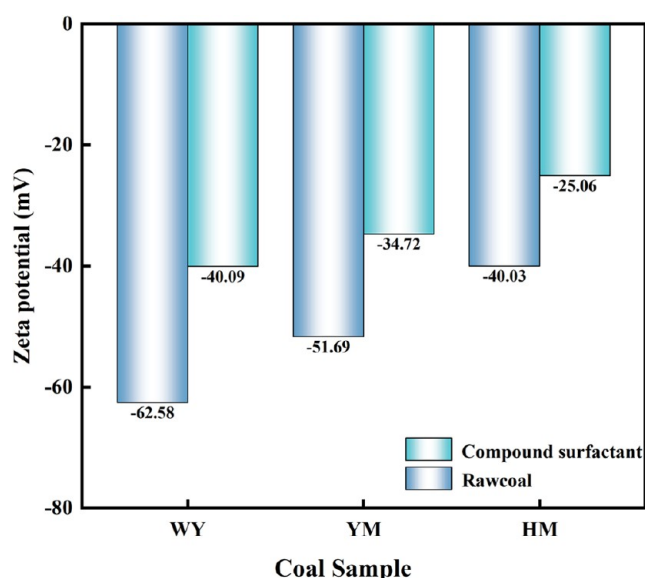


Figure 9. Effect of different system solutions on  $\zeta$ -potential of coal particles.

Table 2. Interaction Energy of Different Systems

different systems	$E_{\text{total}}$ (kcal/mol)	$E_x$ (kcal/mol)	$E_{\text{coal}}$ (kcal/mol)	$E_{\text{int}}$ (kcal/mol)
WY/H <sub>2</sub> O	35028.64	-11847.54	47134.66	-258.48
WY/R1/H <sub>2</sub> O	32427.29	-1211.47	47167.51	-528.74
YM/H <sub>2</sub> O	43614.67	-11716.70	16458.49	-380.32
YM/R1/H <sub>2</sub> O	16814.60	-14116.50	16402.62	-604.66
HM/H <sub>2</sub> O	-12653.86	-1832.88	-320.08	-500.89
HM/R1/H <sub>2</sub> O	-15412.01	-14015.21	-380.64	-1016.16

confined within the range of 0–45 Å. In the anthracite/water system, the relative concentration distribution of coal molecules is less influenced compared to water. The initial water layer distance in this system was 31.75 Å, with an overlap width of 11.51 Å between coal and water. Upon the addition of the R1 composite solution, in the anthracite/R1 composite solution/water system, the initial water layer distance decreased to 4.75 Å, and the overlap width between coal and water expanded to approximately 35.52 Å, an increase of about 24.01 Å compared to the single-water system. Similarly, in the bituminous coal/R1 composite solution/water system, the overlap width increased to 37.21 Å, representing a growth of about 10.34 Å relative to the single-water system. For the lignite/water system, the overlap width between coal and water was 20.33 Å. After incorporating the R1 composite solution, the overlap width in the lignite/R1 composite solution/water system increased significantly to 40.12 Å. The results indicate that the addition of the composite surfactant R1 enhances the overlap width between coal and water, particularly in the lignite/R1 composite system. Surfactant R1 brings water molecules closer to the surface of coal molecules, reduces the starting point of water in the concentration distribution, and expands the overlap range between coal and water.<sup>53</sup> A forward shift in the starting point of the relative concentration distribution of water molecules correlates with a thicker coal/water adsorption layer, deeper penetration of water molecules into coal, and an improved wetting effect on coal. This further demonstrates that the composite surfactant serves as an intermediary between the water layer and coal layer, facilitating the interaction between

water and coal molecules, attracting more water molecules to the coal surface, and enabling deeper penetration of water molecules into coal.

**3.2.3. Analysis of the MSD of Water Molecules.** The MSD and diffusion coefficient ( $D$ ) are effective parameters for characterizing the aggregation behavior of molecules within the system. The equations of motion are presented as follows.

$$D = \frac{1}{6N} \lim_{t \rightarrow \infty} \frac{d}{dt} \sum_{i=1}^N [r_i(t) - r_i(0)]^2 = \frac{1}{6} K_{\text{MSD}} \quad (3)$$

Here,  $N$  represents the total number of diffusing molecules,  $r_i(t)$  and  $r_i(0)$  denote the position vectors of the particles at times  $t$  and 0, respectively, and  $K_{\text{MSD}}$  refers to the slope of the MSD curve.

The MSDs and diffusion coefficients ( $D$ ) of water molecules in various systems are presented in Figure 11 and Table 3, respectively. The results indicate that the MSDs of water molecules exhibit different slopes across the mixing systems, with the smallest slope and  $D$  value observed in the single-water anthracite coal system. This finding suggests that water molecule diffusion in the anthracite system is relatively limited, aligning with previous analyses of interaction energy and relative concentration. Upon the addition of the composite surfactant R1, the diffusion coefficients of coal-composite surfactant–water systems were found to be higher than those of the coal-water system. Specifically, the  $D$  value in the anthracite system increased from  $1.52 \times 10^{-5}$  to  $1.98 \times 10^{-5}$  cm<sup>2</sup>/s, representing a 1.3-fold increase. Similarly, the diffusion coefficients in bituminous coal and lignite systems increased by approximately 1.1–1.2 times after introducing the R1 composite solution. These results demonstrate that the inclusion of composite surfactant molecules attracts more H<sub>2</sub>O molecules toward coal particles, enhancing the interaction energy between the coal surface and water molecules. This phenomenon occurs because surfactant molecules in the composite solution system spontaneously accumulate at the coal/water interface.<sup>54,55</sup> When adsorbed onto the coal surface, the hydrophobic groups of surfactant molecules interact with the coal surface, while their hydrophilic groups extend into the aqueous phase. This redistribution alters the intermolecular force equilibrium at the coal/water interface, reducing surface tension and increasing the number of active sites available for water molecule adsorption. Water molecules are adsorbed onto these active sites through mechanisms such as hydrogen bonding and electrostatic interactions, thereby expanding the active range and mobility of H<sub>2</sub>O molecules. This increased diffusion facilitates the adsorption and penetration of the solution into both the surface and interior of coal particles, ultimately improving the wettability of the coal samples.<sup>56</sup>

## 4. CONCLUSIONS

- (1) Wettability tests indicate that the surfactant blending ratio significantly affects the wetting performance of coal dust. Compared to R2 and R3 composite solutions, the anionic and nonionic composite surfactant (R1) exhibited the most pronounced wetting effect on various coal types at a mass concentration of 0.5 wt % and a mass ratio of 3:2. The R1 composite surfactant achieved a minimum surface tension of 26.246 mN/m, and the minimum contact angles on anthracite, bituminous coal, and lignite were 27.301, 19.575, and 14.545°, respectively. Compared to the monomer solution, the contact angles of the three coal

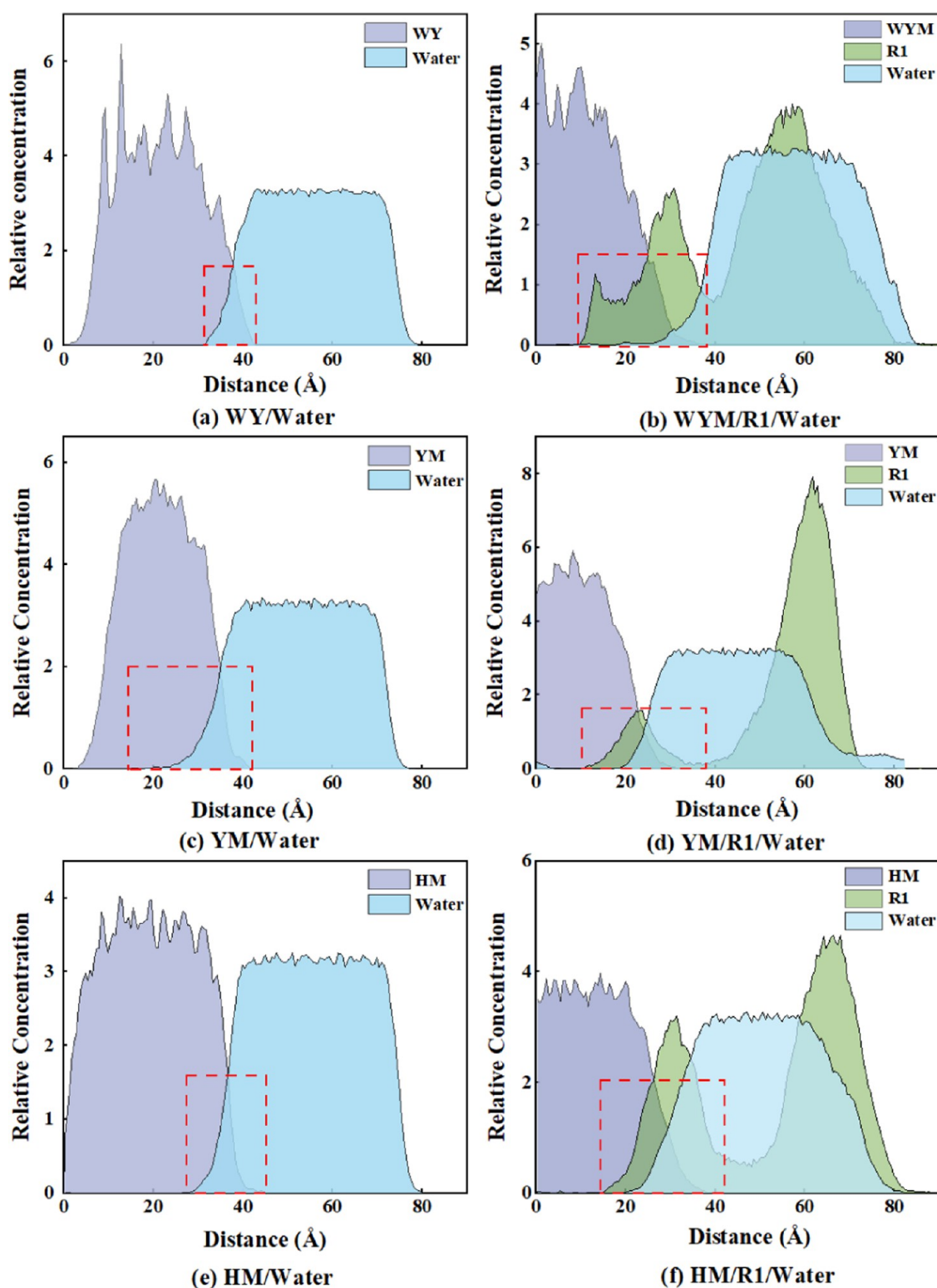
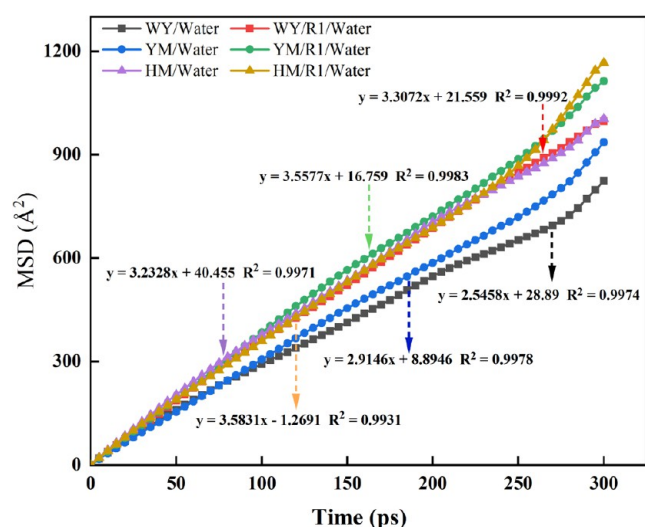


Figure 10. Concentration distribution of components along Z-axis in different systems.

samples treated with the R1 composite surfactant solution decreased by 20.87, 24.29, and 30.17%, respectively, thereby enhancing the wettability of the coal samples.

- (2) The surface morphology and functional group composition of coal changed after treatment with the composite surfactant. Compared to untreated coal, the surfaces of different coal samples treated with the R1 composite surfactant exhibited numerous clusters of coal particles

and increased surface roughness, facilitating aqueous solution penetration for wetting coal dust. The total content of hydrophobic groups ( $-\text{CH}_3$ ,  $-\text{CH}_3\&-\text{CH}_2$ ,  $\text{C}=\text{C}$ ) was significantly reduced, while the total peak area of hydrophilic groups substantially increased. Under the influence of R1 composite surfactant molecules, the absolute values of surface potentials of various coal samples decreased, indicating enhanced aggregation



**Figure 11.** Mean square displacement diagram of water molecules in different systems.

**Table 3.** Diffusion Coefficients for Different Systems

different systems	$D$ ( $10^{-5}$ cm <sup>2</sup> /s)
WY/H <sub>2</sub> O	1.52
WY/R1/H <sub>2</sub> O	1.98
YM/H <sub>2</sub> O	1.75
YM/R1/H <sub>2</sub> O	2.14
HM/H <sub>2</sub> O	1.94
HM/R1/H <sub>2</sub> O	2.15

among coal particles, which promotes dust settling. These findings demonstrate that anionic and nonionic surfactants effectively improve the hydrophilicity of coal samples and enhance coal dust wettability.

- (3) Molecular dynamics simulations further confirmed the effect of the composite surfactant on the wettability of different coal samples. The R1 composite surfactant solution increased the interaction energy within the coal/composite surfactant/water system, resulting in a more stable system and significantly enhanced hydrophilicity. Compared to pure water, the initial positions of water molecules in various systems shifted forward with the addition of the R1 composite surfactant, forming a thicker coal/water adsorption layer. The MSD results of water molecules also indicated that under this ratio, water molecule activity was highest, with diffusion coefficients increasing by approximately 1.1–1.2 times. The enhanced contact probability between water and coal molecules improved the wetting effect.

## ■ ASSOCIATED CONTENT

### SI Supporting Information

The Supporting Information is available free of charge at <https://pubs.acs.org/doi/10.1021/acsomega.4c10578>.

$A_{2924\text{cm}^{-1}}/A_{2954\text{cm}^{-1}}$  peak area ratio of different systems (PDF)

## ■ AUTHOR INFORMATION

### Corresponding Authors

**Limin Du** – College of Safety and Emergency Management Engineering, Taiyuan University of Technology, Taiyuan

030024, China; [orcid.org/0009-0008-5446-0308](https://orcid.org/0009-0008-5446-0308);

Email: [2470417542@qq.com](mailto:2470417542@qq.com)

**Jun Nian** – College of Safety and Emergency Management Engineering, Taiyuan University of Technology, Taiyuan 030024, China; Postdoctoral Workstation, Shanxi Coking Coal Group Co., LTD., Taiyuan, Shanxi 030021, China; Email: [nianjun@tyut.edu.cn](mailto:nianjun@tyut.edu.cn)

## Authors

**Jinqi Fu** – College of Safety and Emergency Management Engineering, Taiyuan University of Technology, Taiyuan 030024, China

**Jingchi Zhu** – College of Safety and Emergency Management Engineering, Taiyuan University of Technology, Taiyuan 030024, China

**Hongfei Yu** – College of Safety and Emergency Management Engineering, Taiyuan University of Technology, Taiyuan 030024, China

**Xiaoxia He** – College of Safety and Emergency Management Engineering, Taiyuan University of Technology, Taiyuan 030024, China

**Chaowei Yang** – College of Safety and Emergency Management Engineering, Taiyuan University of Technology, Taiyuan 030024, China

**Lei Zhang** – College of Safety and Emergency Management Engineering, Taiyuan University of Technology, Taiyuan 030024, China

Complete contact information is available at:

<https://pubs.acs.org/10.1021/acsomega.4c10578>

## Author Contributions

<sup>§</sup>L.D. and J.N. contributed equally to this work. L.D.: Writing—original draft, Methodology, Project administration, Conceptualization. J.N.: Methodology, Funding acquisition. J.F.: Project administration. J.Z.: Resources. H.Y.: Visualization. X.H.: Investigation. C.Y.: Software. L.Z.: Supervision.

## Notes

The authors declare no competing financial interest.

## ■ ACKNOWLEDGMENTS

This work was financially supported by the National Natural Science Foundation of China (52274220), which is gratefully acknowledged.

## ■ REFERENCES

- (1) Shen, Y.; Gu, Z. M.; Wang, C. Phase transformation behaviors in the heat-affected zones of ferritic heat-resistant steels enabled by in situ cslm observation. *Acta Metall. Sin.* **2024**, *60* (6), 802–816.
- (2) Shang, M.; Peng, M. Y. P.; Peng, M. Y.; Anser, M. K.; Anser, M. K.; Imran, M.; Nassani, A. A.; Binsaeed, R. H. Evaluating the u-shaped environmental kuznets curve in china: the impact of high technology exports and renewable energy consumption on carbon emissions. *Gondwana Res.* **2024**, *127*, 272–287.
- (3) Sun, Y.; Wen, G.; Dai, H.; Feng, Y.; Azaele, S.; Lin, W.; Zhou, F. Quantifying the resilience of coal energy supply in china toward carbon neutrality. *Research* **2024**, *7*, No. 0398, DOI: [10.34133/research.0398](https://doi.org/10.34133/research.0398).
- (4) Xu, Z.; Zhang, T.; Zhuang, L.; Wu, P.; Lu, C. The impact of coal-fired, soot on china's industrial production and total factor energy efficiency. *Water, Air, Soil Pollut.* **2024**, *235* (9), No. 565, DOI: [10.1007/s11270-024-07366-0](https://doi.org/10.1007/s11270-024-07366-0).
- (5) Lu, C.; Li, P.; Xu, J.; Chai, J. Knowledge map analysis of coal mine water disaster prevention and control in china from 2000 to 2023. *Earth Sci. Inf.* **2024**, *17* (4), 2791–2799.

- (6) Zhang, G.; Wang, E. Risk identification for coal and gas outburst in underground coal mines: a critical review and future directions. *Gas Sci. Eng.* **2023**, *118*, No. 205106, DOI: 10.1016/j.gjsce.2023.205106.
- (7) Dong, S.; Wang, H.; Guo, X.; Zhou, Z. Characteristics of water hazards in china's coal mines: a review. *Mine Water Environ.* **2021**, *40* (2), 325–333.
- (8) Lu, Y.; Li, X. A study on a new hazard detecting and controlling method: the case of coal mining companies in china. *Saf. Sci.* **2011**, *49* (2), 279–285.
- (9) Liang, Y.; Shi, B.; Yue, J.; Zhang, C.; Han, Q. Anisotropic damage mechanism of coal seam water injection with multiphase coupling. *ACS Omega* **2024**, *9* (14), 16400–16410.
- (10) Zan, Y.; Wu, Y.; Ran, D.; Wang, J.; Chen, Q.; Lu, H.; Huang, Z. Nano-emulsion stabilized by multiple surfactants: an effective alternative for enhancing coal seam water injection effect. *J. Mol. Liq.* **2024**, *398*, No. 124150, DOI: 10.1016/j.molliq.2024.124150.
- (11) Huang, L.; Li, B.; Wu, B.; Li, C.; Wang, J.; Cai, H. Study on the extension mechanism of hydraulic fractures in bedding coal. *Theor. Appl. Fract. Mech.* **2024**, *131*, No. 104431, DOI: 10.1016/j.tafmec.2024.104431.
- (12) Gao, M.; Li, H.; Zhao, Y.; Liu, Y.; Zhou, W.; Li, L.; et al. Mechanism of micro-wetting of highly hydrophobic coal dust in underground mining and new wetting agent development. *Int. J. Min. Sci. Technol.* **2023**, *33* (1), 31–46.
- (13) Zhang, Z.; Yang, J.; Qi, R.; Huang, J.; Chen, H.; Zhang, H. Development of hydrophobic coal-fly-ash-based ceramic membrane for vacuum membrane distillation. *Materials* **2023**, *16* (8), No. 3153, DOI: 10.3390/ma16083153.
- (14) Bao, L.; Yang, Y.; Li, J.; Li, X.; Dong, J. Synthesis and structure-property relationship of coal-based isomeric alkylbenzene sulfonate surfactants. *Colloids Surf., A* **2024**, *696*, No. 134350, DOI: 10.1016/j.colsurfa.2024.134350.
- (15) Liu, H.; Li, Z.; Zheng, C.; Wang, Y.; Song, F.; Meng, X. Wettability characteristics of low-rank coals under the coupling effect of high mineralization and surfactants. *ACS Omega* **2023**, *8*, 39004–39013, DOI: 10.1021/acsomega.3c03583.
- (16) Silva, S. C. M.; Gambaryan-Roisman, T.; Venzmer, J. Surface tension behavior of superspreading and non-superspreading trisiloxane surfactants. *Colloid Polym. Sci.* **2023**, *301* (7), 739–744.
- (17) Guzman-Valencia, C. J.; Toriz-Salinas, J.; Espinosa-Jimenez, H.; Salazar-Arriaga, A. B.; Lopez-Cervantes, J. L.; Dominguez, H. Understanding the surface tension reduction of the water/air interface due to the synergistic effect of the sds-ctab mixture: a molecular dynamics simulation study. *Mol. Phys.* **2024**, *122*, No. e2375041, DOI: 10.1080/00268976.2024.2375041.
- (18) Wang, K.; Xu, M.; Zhou, B.; Yang, M.; Liu, R. Study on the effects of inorganic salts and ionic surfactants on the wettability of coal based on the experimental and molecular dynamics investigations. *Energy* **2024**, *300*, No. 131610, DOI: 10.1016/j.energy.2024.131610.
- (19) Wang, X.-H.; Jiang, B.; Yuan, L.; Zhao, Y.; Yu, C.; Zheng, Y.; et al. Study on coupling chelating agent and surfactant to enhance coal wettability: experimental and theoretical discussion. *Fuel* **2023**, *342*, No. 127861, DOI: 10.1016/j.fuel.2023.127861.
- (20) Xu, L.; Li, Y.; Du, L.; Yang, F.; Zhang, R.; Wei, H.; et al. Study on the effect of sds and sds on deep coal seam water injection. *Sci. Total Environ.* **2022**, *856*, No. 158930, DOI: 10.1016/j.scitotenv.2022.158930.
- (21) Bai, X.; Kong, S.; Zhang, J.; Li, G.; Li, J.; Wen, P.; Yan, G. Molecular mechanism study of nonionic surfactant enhanced anionic surfactant to improve the wetting ability of anthracite dust. *Colloids Surf., A* **2024**, *686*, No. 133455, DOI: 10.1016/j.colsurfa.2024.133455.
- (22) Niu, W.; Nie, W.; Yuan, M.; Bao, Q.; Zhou, W.; Yan, J.; et al. Study of the microscopic mechanism of lauryl glucoside wetting coal dust: environmental pollution prevention and control. *J. Hazard. Mater.* **2021**, *412*, No. 125223, DOI: 10.1016/j.jhazmat.2021.125223.
- (23) Li, J.; Kong, S.; Yan, G.; Chen, X. Adsorption mechanism of alkylphenol ethoxylates surfactants (apeo) on anthracite surface: a combined experimental, dft and molecular dynamics study. *J. Mol. Liq.* **2024**, *396*, No. 124030, DOI: 10.1016/j.molliq.2024.124030.
- (24) Tian, Q.; Nie, W.; Bao, Q.; Niu, W.; Li, R.; Zhang, X.; et al. Research on coal dust pollution prevention and control based on co-solvent association: macro-micro experiments and molecular dynamics simulations. *Appl. Surf. Sci.* **2024**, *651*, No. 159289, DOI: 10.1016/j.apsusc.2024.159289.
- (25) Guo, J.; Zhang, L.; Liu, S.; Li, B. Effects of hydrophilic groups of nonionic surfactants on the wettability of lignite surface: molecular dynamics simulation and experimental study. *Fuel* **2018**, *231*, 449–457.
- (26) Liu, H.; Li, R.; Nie, W.; Bao, Q.; Niu, W.; Tian, Q.; Zhang, X. Enhancing understanding of anionic surfactant adsorption mechanism and hydrophilic modification of bituminous coal for effective dust suppression. *Surf. Interfaces* **2024**, *46*, No. 103948, DOI: 10.1016/j.surfin.2024.103948.
- (27) Chen, X.; Zuo, P.; Zhang, G.; Min, R.; Zhao, S. Study of the micromechanism of the effect of fatty alcohol poly(oxyethylene) ether-9 on the wettability of jincheng anthracite. *ACS Omega* **2022**, *7* (46), 42582–42592.
- (28) Sun, L.; Ge, S.; Chen, X.; Liu, S. Study on atomization and dust reduction mechanisms of aeo-9-charged solution. *Energies* **2023**, *16* (6), No. 2800, DOI: 10.3390/en16062800.
- (29) Liu, B.; Lei, X.; Ahmadi, M.; Jiang, L.; Chen, Z. Surface modeling of wettability transition on  $\alpha$ -quartz: insights from experiments and molecular dynamics simulations. *J. Mol. Liq.* **2024**, *406*, No. 125147, DOI: 10.1016/j.molliq.2024.125147.
- (30) Jiang, C.; Fei, Z.; Ma, Z.; Liu, X.; Niu, J.; Hou, Y. Hydrophilic-hydrophobic heterogeneous interface enables the formation of a high-performance polyamide membrane for water purification. *Sep. Purif. Technol.* **2023**, *316*, No. 123752, DOI: 10.1016/j.seppur.2023.123752.
- (31) Meng, J.; Wang, L.; Lyu, C.; Wang, J.; Lyu, Y.; Nie, B. Molecular simulation of the regulation mechanism of the hydrophilic structure of surfactant on the wettability of bituminous coal surface. *J. Mol. Liq.* **2023**, *383*, No. 122185, DOI: 10.1016/j.molliq.2023.122185.
- (32) Zhou, L.; Yang, S.; Hu, B.; Yuan, Z.; Wu, H.; Yang, L. Evaluating of the performance of a composite wetting dust suppressant on lignite dust. *Powder Technol.* **2018**, *339*, 882–893.
- (33) Jia, H.; Song, J.; Sun, Y.; Xu, M.; Li, C.; Wei, Z.; et al. Novel molecular insights into the effects of ethoxy group number on emulsification and viscosity reduction of anionic-nonionic surfactants. *Energy Fuels* **2023**, *37* (20), 15615–15625.
- (34) Hou, J.; Lin, S.; Du, J.; Sui, H. Study of the adsorption behavior of surfactants on carbonate surface by experiment and molecular dynamics simulation. *Front. Chem.* **2022**, *10*, No. 847986, DOI: 10.3389/fchem.2022.847986.
- (35) Jing, D.; Bao, C.; Dong, Z.; Meng, X.; Han, X.; Li, G.; Chen, J. Study on the compounding optimization of surfactants and synergistic effects on the wettability of bituminous coal. *Sci. Rep.* **2024**, *14* (1), No. 11461, DOI: 10.1038/s41598-024-61266-1.
- (36) Xu, Y.-L.; Huo, X.; Wang, L.; Gong, X.; Lv, Z.; Zhao, T. Study of the microstructure of coal at different temperatures and quantitative fractal characterization. *ACS Omega* **2023**, *8* (25), 23098–23111.
- (37) Isah, U. A.; Rashid, M. I.; Lee, S.; Kiman, S.; Iyodo, H. M. Correlations of coal rank with the derived fourier transform infra-red (ftir) spectroscopy structural parameters: a review. *Infrared Phys. Technol.* **2024**, *141*, No. 105456, DOI: 10.1016/j.infrared.2024.105456.
- (38) Ni, X.; Feng, D.; Liu, Y.; Han, L. Coal wetting characteristics and mechanism of water with different degrees of mineralization. *Energy Fuels* **2024**, *38* (21), 20644–20652.
- (39) Zhang, K.; Zhang, Y.; Zhou, L.; Li, H.; Shi, W.; Cheng, X.; et al. Experimental and theoretical insight into the effect of a novel composite dispersant on the properties of coal pitch water slurry. *Fuel* **2024**, *365*, No. 131281.
- (40) Gao, F.; Jia, Z.; Cui, Z.; Li, Y.; Jiang, H. Evolution of macromolecular structure during coal oxidation via ftir, xrd and raman. *Fuel Process. Technol.* **2024**, *262*, No. 108114, DOI: 10.1016/j.fuproc.2024.108114.
- (41) Wang, K.; Pan, J.; Wang, E.; Hou, Q.; Yang, Y.; Wang, X. Potential impact of co<sub>2</sub> injection into coal matrix in molecular terms. *Chem. Eng. J.* **2020**, *401*, No. 126071, DOI: 10.1016/j.cej.2020.126071.

- (42) Wu, M.; Li, H.; Wang, J.; Wang, L.; Li, S.; Wang, Y.; et al. Inhibitory performance and mechanism analysis of modified fly-ash inhibitor on the coal spontaneous combustion: a combined study of laboratory experiments and molecular dynamic simulation. *Process Saf. Environ. Prot.* **2025**, *193*, 313–326.
- (43) Hehe, J.; Guanhua, N.; Chuanjie, Z.; Xiangfei, Z.; Gongshuai, S.; Zhenyang, W.; Qiming, H. Molecular dynamics simulations and experimental characterization of the effect of different concentrations of [bmim][cl] in aqueous solutions on the wettability of anthracite. *Fuel* **2022**, *324*, No. 124618, DOI: 10.1016/j.fuel.2022.124618.
- (44) Wang, S.; Shi, S.; Jiang, B.; Zheng, Y.; Yu, C.; Zhang, Y.; Wang, X. H. Influence of surfactant adsorption on coal oxidation and wettability: experimental discussion and model development. *Energy* **2024**, *297*, No. 131304, DOI: 10.1016/j.energy.2024.131304.
- (45) Ai, C.; Liu, S.; Zhao, S.; Mu, X.; Jia, Z. An investigative and simulative study on the wetting mechanism of alkaline dust suppressant acting on long-flame coal. *Sci. Rep.* **2024**, *14* (1), No. 26794.
- (46) Dwivedi, A.; Dwivedi, A.; Kumar, A. Qualitative surface characterization of indian permian coal using xps and ftir. *Int. J. Coal Prep. Util.* **2023**, *43* (7), 1152–1163.
- (47) Chen, C.; Tang, Y.; Guo, X. Comparison of structural characteristics of high-organic-sulfur and low-organic-sulfur coal of various ranks based on ftir and raman spectroscopy. *Fuel* **2022**, *310*, No. 122362, DOI: 10.1016/j.fuel.2021.122362.
- (48) Ji, B.; Jiang, B.; Yuan, L.; Zhou, Y.; Wang, H.; Tao, W.; Zhang, Y. Effect of side chain functional groups of ionic liquids on improving wettability of coal: simulation and experimental discussion. *Energy* **2023**, *285*, No. 129543.
- (49) Li, L.; Li, Z.; Zhu, X.; He, M.; Ma, C.; Wang, Q.; et al. Theoretical calculation and experimental investigation on ionic liquid [c 16 mim]cl affecting wettability of low-rank coal. *Adv. Compos. Hybrid Mater.* **2022**, *5* (2), 1241–1252.
- (50) Ji, B.; Jiang, B.; Yuan, L.; Yu, C.; Zhou, G.; Zhao, Y.; et al. Experimental and molecular dynamics simulation study on the influence of sds and jfc composite ratios on bituminous coal wettability. *Process Saf. Environ. Prot.* **2023**, *174*, 473–484.
- (51) Yu, X.; Hu, X.; Zhao, Y.; et al. Molecular dynamics simulation of interface adhesion characteristics between dust suppressant and coal. *Mater. Today Commun.* **2022**, *33*, No. 104487, DOI: 10.1016/j.mtcomm.2022.104487.
- (52) Bao, Q.; Xu, J.; Nie, W.; Niu, W.; Tian, Q.; Yuan, M. Simulation study of the mechanism of mesoscopic adsorption and the evolution of molecular dynamics of a surfactant/polymer composite on the surface of low rank coal. *J. Mol. Graphics Modell.* **2022**, *116*, No. 108276, DOI: 10.1016/j.jmgm.2022.108276.
- (53) Zhao, Z.; Li, Y.; Zhang, Z. Effect of surfactant on the attachment between coal particles and bubbles: an experimental and molecular dynamics simulation study. *Fuel* **2023**, *337*, No. 127272, DOI: 10.1016/j.fuel.2022.127272.
- (54) Zhou, G.; Xing, M.; Wang, K.; Wang, Q.; Xu, Z.; Li, L.; Cheng, W. Study on wetting behavior between ctac and bs-12 with gas coal based on molecular dynamics simulation. *J. Mol. Liq.* **2022**, *357*, No. 118996, DOI: 10.1016/j.molliq.2022.118996.
- (55) Zhang, Q.; Wang, B.; Xing, X.; Li, J.; Wang, Z. Wetting characteristics and kinetic behavior of amphoteric ionic surfactant on the microscopic "solid-liquid" interface of coal - a case study. *J. Mol. Liq.* **2023**, *392*, No. 123497.
- (56) Zhang, Q.; Wang, B.; Zhou, G.; et al. Research on the microstructure construction and the "solid-liquid" interface wetting mechanism of variable rank coal macromolecules. *J. Mol. Struct.* **2025**, *1326*, No. 141161, DOI: 10.1016/j.molstruc.2024.141161.